Performance Characteristics of a Model VTOL Lift Fan in Crossflow

S. Lieblein,* J. A. Yuska,† and J. H. Diedrich‡
NASA Lewis Research Center, Cleveland, Ohio

This paper presents a summary of principal results obtained from crossflow tests of a model 15-in.-diam lift fan installed in a wing in the NASA Lewis Research Center, 9 × 15 ft V/STOL Propulsion Wind Tunnel. Tests were run with and without exit louvers over a range of tunnel air speeds, fan speeds, and wing angle of attack. Fan thrust in crossflow was influenced by two principal factors: the effects of inflow distortion on blade-row performance; and changes in fan stage operating point brought about by changes in back pressure ratio. In this particular fan, flow separation on the inlet bellmouth did not appear to be a serious problem for crossflow operation.

Introduction

THE high-bypass-ratio lift fan is currently a prime candidate for the lift propulsion system for V/STOL transport aircraft. Numerous studies have indicated the potential feasibility of lift-fan V/STOL aircraft, and many experimental investigations have shown acceptable performance characteristics for fan aircraft configurations. A recent review of lift fan propulsion for civil V/STOL transports is contained in Ref. 1.

From the propulsion point of view, an important question is the influence of the crossflow velocity on the basic performance of the fan. Of particular concern is the effect of flow distortions and interactions that operate on both the inlet and outlet flows of the fan during the transition from the vertical to the horizontal flight mode.[2] Such crossflow-induced interactions can have significant effects on fan operating point, thrust and noise levels, and efficiency.

The potential adverse effects of the crossflow component on the flow into the fan inlet have been well documented in a number of studies (e.g., Refs. 3-11). These investigations have revealed the presence of boundary-layer separation on the inlet bellmouth surfaces and circumferential variations in flow components at the face of the fan rotor under crossflow conditions. However, comparatively little experimental or analytical information has appeared on possible outlet flow interactions or on the detailed nature of the response of a fan stage to inlet and outlet distortions during transition.

This paper presents a summary of the principal results obtained from crossflow tests of a 15-in.-diam lift fan with extensive internal instrumentation installed in a wing in a wind tunnel. The basic objective of the investigation was to determine lift fan behavior in the crossflow environment and to define the principal factors affecting fan performance.

Apparatus

A 15-in.-diam model lift fan was installed in a 9- × 4.5-ft wing and tested in the NASA Lewis Research Center 9- × 15-ft V/STOL Propulsion test tunnel, as shown in Fig. 1. The wing had a constant airfoil section with a maximum thickness ratio of 17% [modified NACA 65_3A(218)-217 section]. The model lift fan was installed at midspan with its axis located at the 40% chord position. Remote actuation of the wing assembly was available over a range of geometric angle of attack from −15° to +15°. However, during static tests (no crossflow), the wing was located with its chord perpendicular to the axis of the test section (−90°) to eliminate flow recirculation effects. Descriptive details of the test tunnel are given in Ref. 12.

A cross section of the lift fan assembly is shown in Fig. 2. The fan rotor was driven by a compact two-stage supersonic turbine located in the hub section of the assembly. This arrangement provided for coaxial exhaust streams. High-pressure air to drive the turbine was supplied through six equally-spaced 12%-thick struts spanning the fan passage. These struts also served as the structural support for the inner components of the assembly.

Four louver vanes for aft flow deflection were attached to the wing with remote actuation from a vane chord position of −2.5° to +40° from the fan axis. The exit louvers were 8%-thick airfoil sections (NACA 63-series, 0.6 lift coefficient) with a solidity of 1.25 and aspect ratio of 3.3.

The rotor tip leading edge was located 2.4 in. axially from the peak height of the forward point of the inlet bellmouth. This provided for a ratio of inlet depth to rotor tip diameter of 0.16. Two 0.060-in.-diam damper wires were located on the rotor blades at 60% of the passage height from the hub to reduce blade vibration and prevent blade flutter in crossflow. The axial spacing between rotor and stator blades was approximately 0.75 in.

The inlet bellmouth was designed according to the method described in Ref. 13 to avoid velocity peaks on the outer shroud during static (no crossflow) operation. The fan stage was designed according to the general approach of Ref. 14. Specific fan stage design characteristics were: over-all pressure ratio, 1.28; corrected tip speed, 980 fps;

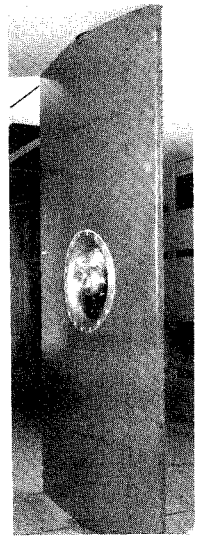

Fig. 1 The 15-in.-diam fan-in-wing model installed in the Lewis Research Center 9 by 15 ft V/STOL test section.

Received November 8, 1971; revision received December 26, 1972.
Index categories: VTOL Propulsion; VTOL Testing.
*Chief, VTOL Propulsion Branch. Associate Fellow AIAA.
†Project Engineer, VTOL Performance Section. Member AIAA.
‡Head, VTOL Performance Section. Member AIAA.

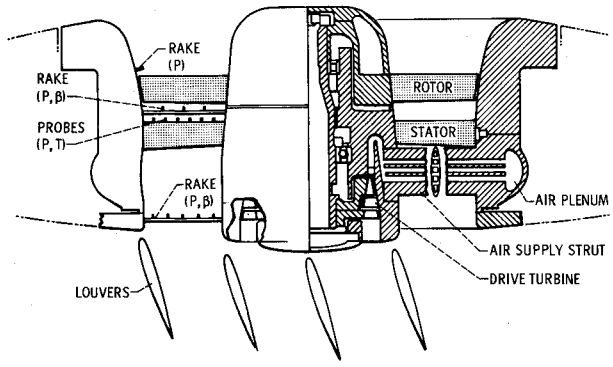

Fig. 2 Cross section of 15-in. model lift fan.

corrected weight flow, 39.8 lb/sec (M = 0.60); inlet total pressure, 2116 lb/ft^2; inlet total temperature. 80°F; exit static pressure, 2116 lb/ft^2; axial thrust, 810 lb; and power input, 580 hp. The rotor blades were double circular arc sections with aspect ratio of 2.6, hub-tip ratio of 0.463, and tip solidity of 1.25. The stator blades were NACA 65-series sections with aspect ratio of 3 and tip solidity of 1.0.

The major features of the fan internal instrumentation are shown in Fig. 2. For the inlet bellmouth, static taps were spaced along the surface at eight circumferential positions on the outer shroud. Three 0.25-in.-long wall rakes, each with four total pressure probes, were placed at three circumferential positions on the forward half of the inlet 0°, −55°, and +55°) and approximately 0.5 in. forward of the rotor leading edge.

Six fixed-position rakes were equally spaced around the circumference to measure flow angle and total pressure at the outlet of both the rotor and the duct. In addition, six stators were each instrumented with total temperature probes. Static taps were located at six equally-spaced positions on the hub and tip surfaces in the measuring plane of the total pressure probes at both rotor and duct exit. Turbine mass flow rate and inlet and exit total temperature were also determined, and base static pressures were measured on the ring between the fan and turbine flow passages and on the centerbody surface of the turbine.

Performance Variations

The over-all crossflow performance of the fan assembly, consisting of the fan stage, drive turbine, and inlet bellmouth, is shown in Fig. 3. Data are presented at rotor corrected design tip speed (980 fps) for total corrected thrust, F/δ, and drive-turbine power output, $hp/\delta(\theta)^{1/2}$, both expressed as a ratio of the frontal area of the fan, A, (rotor tip diam = 15.2 in.). The total thrust was computed as the sum of the fan discharge and turbine discharge thrusts and the net force on the inner base of the turbine. This value represents the total thrust available at the exit of the fan.

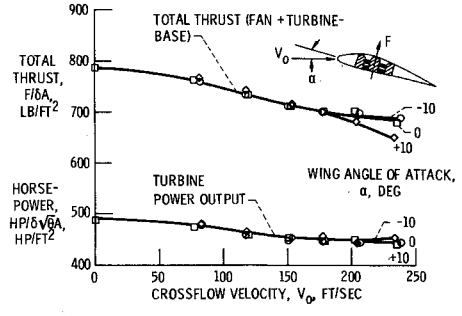

Fig. 3 Over-all performance of fan assembly in crossflow—louvers off; design tip speed, 980 fps.

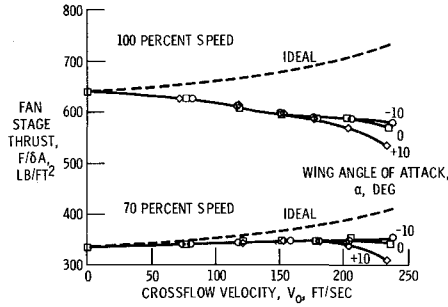

Fig. 4 Thrust of fan stage in crossflow—louvers off.

In Fig. 3, both fan total thrust and power input tended to decrease with increasing crossflow velocity. Angle of attack started to become a variable at the high values of crossflow velocity. At a cross-flow velocity of 240 fps (164 mph) and zero-degree wing angle of attack, the total thrust decreased by around 12.5% compared to the zero-crossflow value.

The variation of thrust from the discharge of the fan stage is shown in Fig. 4 for 70 and 100% design speed conditions. At design speed, as in the case of the total thrust, the fan stage thrust decreased with increasing crossflow velocity. At 70% speed, however, stage thrust tended to rise slightly, except for the high-angle-of-attack configuration. In all cases, increased wing angle of attack at high crossflow velocities resulted in a reduction of fan stage thrust. At zero angle of attack and design speed, the decrease in fan stage thrust at 240 fps was around 11% compared to a decrease of around 12.5% for the total thrust (Fig. 3). Thus, the behavior of the fan stage thrust can be taken as a valid measure of the variation of the total thrust.

Also shown for comparison in Fig. 4 is the variation in ideal fan stage thrust computed assuming complete recovery of the momentum of the crossflow entering the fan (i.e., ambient total pressure increases with increasing crossflow velocity, inlet pressure losses are zero, total pressure ratio across the stage remains constant, and outlet static pressure is the ambient value). The deviation from ideal fan thrust is considerably greater at the higher tip speed than at the lower tip speed.

Since fan stage thrust is determined primarily by exit total pressure and mass flow rate, it was of interest to examine the crossflow variations of these parameters. Figure 5 shows the variation of average exit total pressure ratio at 100 and 70% design speed. Corresponding variations in calculated fan stage flow rate revealed only a modest decrease in flow rate with crossflow velocity at design tip speed. At 70% design speed, there was a slight rise in flow rate over the initial crossflow velocity range. Increasing angle of attack had a marked effect in reducing fan flow rate only at crossflow velocities greater than around 180 fps at both tip speed levels. It appeared therefore, that

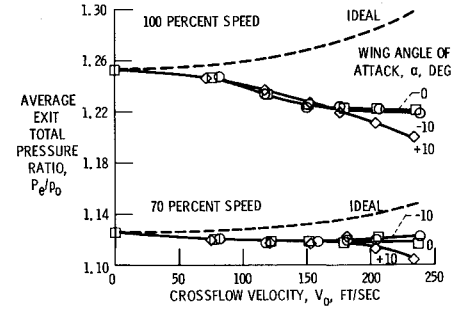

Fig. 5 Fan duct exit total pressure ratio in crossflow—louvers off.

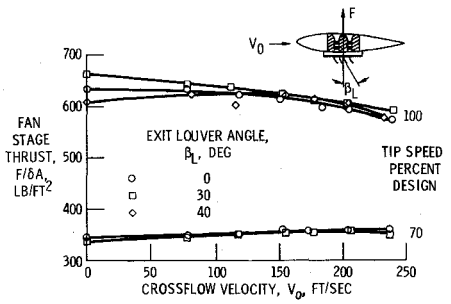

Fig. 6 Thrust of fan stage with exit louvers on wing—zero wing angle of attack.

the crossflow variation of stage thrust (Fig. 4) was the result primarily of the crossflow variation of exit total pressure ratio (Fig. 5).

The influence of exit louvers on the thrust of the fan stage is shown in Fig. 6 for two tip speed conditions. At design speed, variations in louver angle had a significant effect on stage thrust only at zero or low crossflow velocities. No significant effect of louver position appeared at the low tip speed. As will be discussed later, the variations in stage thrust reflected the effects of louver-induced variations of back pressure on the operating point of the fan stage.

Internal Flow Distributions

Inlet Bellmouth

Previous inlet experiments and theory have indicated that substantial circumferential and radial variations in velocity and angle will occur during crossflow conditions at the entrance to a fan rotor row that is installed in a shallow inlet. The nature of this inlet distortion effect is illustrated in Fig. 7. In crossflow, the inflow velocity is increased over the forward portion of the bellmouth and decreased over the aft portion. At the same time, the incomplete turning of the air results in an advancing/retreating blade motion with respect to the incoming air. These two factors result in a circumferential variation in incidence angle, i, on the rotor blade. Roughly, negative incidence angles might be expected from around 315°–135°, and positive incidence angles from around 135°–315°. This form of inlet flow distortion is a potential flow phenomenon.

On the surfaces of the inlet bellmouth, the forward portion of the outer shroud and the aft portion of the nosepiece would experience pronounced accelerating and decelerating flows resulting from the surface curvatures. For the practical range of crossflow velocities and inlet bellmouth depths, these surface velocity gradients can lead to local boundary-layer separation at the inlet to the rotor. This form of inlet distortion is a viscous flow phenomenon. These viscous and potential forms of inlet distortion were clearly present in the inlet of the model life fan tested.

The variation in static pressure along the surface of the bellmouth, p_s, at 10° from the full forward position is illustrated in Fig. 8. Values of surface velocity above the sonic value were attained at crossflow velocities as low as 120 fps. Evidence of boundary-layer separation was found on the inlet wall rake located at the 0° position. However, no separation was noted by the rakes at −55° or +55° for any of the test variables covered. Boundary-layer separation appeared to be restricted to a relatively small area of the forward portion of the bellmouth.

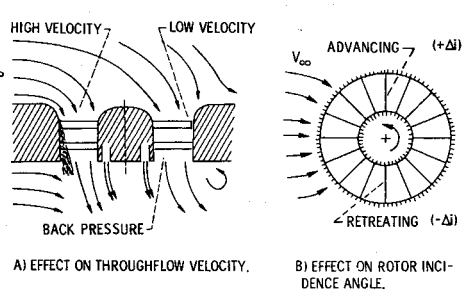

Fig. 7 Lift fan inflow in crossflow.

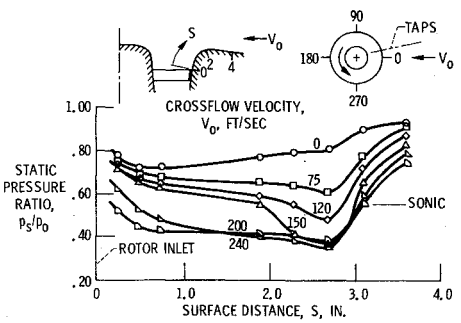

Fig. 8 Pressure variation on bellmouth surface—10° position; zero angle of attack.

The total pressure profiles of the three inlet wall rakes, along with a comparison of weight flow rates determined from duct outlet measurements and correlations for inlet weight flow established from potential flow calculations, were used to estimate the percent blockage of the inlet annulus area due to boundary-layer buildup. The results are shown in Fig. 9 for 100% and 70% design speed. Attainment of separation at the forward position (θ = 0°) is indicated by the dashed line in Fig. 9. As might be expected, an increasing trend with both crossflow velocity and angle of attack was found.

The average loss in total pressure involved in the localized separated flow region model as sketched in Fig. 9 was estimated to be less than 1% for the worst case (100% speed and +10° angle of attack). Thus, the viscous loss effects associated with this particular bellmouth design are not likely to pose any serious problem for crossflow operation.

Fan Stage

As indicated earlier in the discussion of Fig. 7, the distortion of the freestream flow in the inlet bellmouth in crossflow tends to produce a circumferential variation in incidence angle on the fan rotor. These changes in incidence angle Δi should produce circumferential variations in total pressure rise. An example of total pressure ratio P_2/p_0 measured around the outlet of the rotor at the mid-radius position at design tip speed is given in the upper part of Fig. 10. Reduced total pressure was observed at the 90° position, and increased total pressure was observed at the 270° position as crossflow velocity was in-

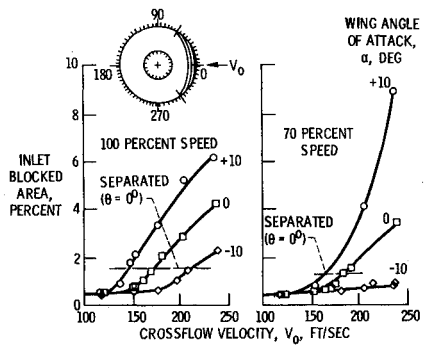

Fig. 9 Estimated rotor inlet-area blockage due to bellmouth surface boundary layer.

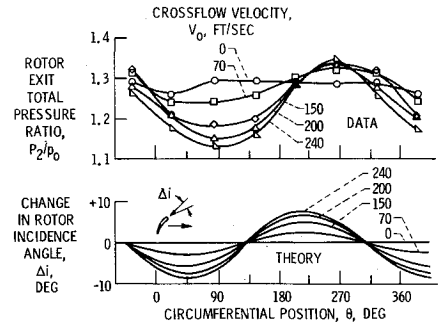

Fig. 10 Rotor outlet total pressure in crossflow—midpassage radius; design tip speed.

creased. For the highest crossflow velocity test condition, the variation from minimum pressure ratio to maximum pressure ratio was quite large (1.13–1.35).

Theoretical variations of change in rotor incidence angle, Δi, with circumferential position θ from potential flow theory (method of Ref. 15) for the midradius position at design conditions are shown on the lower part of Fig. 10. The measured circumferential variation in outlet total pressure ratio shows essentially the same trend as the theoretical change in incidence angle. However, peak variations in total pressure were shifted by around 45° in the direction of fan rotation from the peaks of the change in incidence angle.

Unlike the theoretical incidence variations, the peak measured total pressure ratio (at 270°) did not continue to rise with increasing crossflow velocity to the same degree that the minimum pressure decreased (at 90°). In fact, only a small increase in peak total pressure was noted as crossflow velocity increased from 70 fps to 240 fps. It may be that some form of local stall condition was reached as local incidence angle was increased, or that the crossflow altered the effective operating point of the fan through changes in the back pressure of the stage. As a consequence of the local variations, the average total pressure over the circumference tended to decrease in crossflow. Specifically, the average rotor outlet total pressure ratio P_2/p_0 at midradius decreased from a value of 1.28 at zero crossflow to a value of 1.22 at 240 fps.

An example of flow angle measured at the outlet of the rotor, β_2, at the midradius position at design tip speed is given in the upper part of Fig. 11. The test data show maximum angles at around 100° and minimum angles at around 280°. The maximum variations in angle approached 12° at a crossflow velocity of 240 fps.

The lower part of Fig. 11 shows the calculated variation of absolute flow angle at the inlet to the rotor, β_1, at midradius as obtained from potential flow theory. The form of the theoretical inlet variation is strikingly similar to the

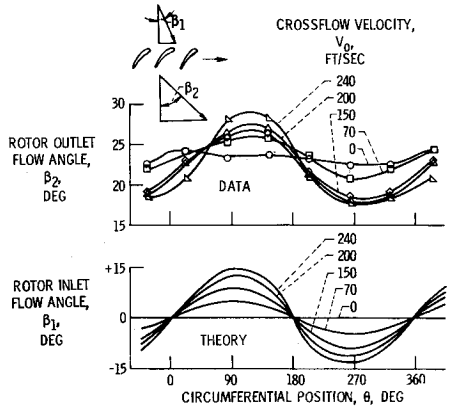

Fig. 11 Rotor flow angle in crossflow-midpassage radius; design tip speed.

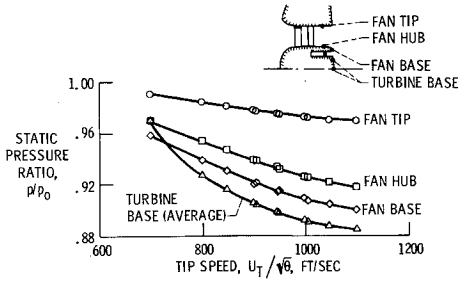

Fig. 12 Exit static pressures—louvers off; no crossflow.

measured outlet variation, although the magnitude of angle change is substantially greater (30° difference for theory vs 12° for data). This difference in magnitude may be the result of the contributing effect of the circumferential variation of rotor pressure rise on change in local angle across the rotor.

The circumferential variation of flow angle at the rotor outlet, β_2, (upper part of Fig. 11) represents a distortion of the freestream flow entering the stator. If the stator is designed for minimum-loss setting angle for the static case (no crossflow), then excursions in inlet angle represent departures from minimum-loss incidence angle. Local increases in total pressure loss can then occur across the stator, depending upon the basic design and loss characteristics of the blade elements of the stator.

A significant decrease in average total pressure ratio was observed from the rotor exit to the duct exit. This pressure drop tended to increase with increasing crossflow velocity. However, it should be noted that the measured loss in average total pressure ratio from rotor outlet to duct outlet was due to duct losses and to mixing losses from the rotor damper wires as well as to losses across the stator blades.

The circumferential flow variations in crossflow observed at the rotor exit were found to persist through to the exit of the duct. There was some change in the form of the circumferential distribution of the outlet angle, but the general variation in total pressure at the duct exit was quite similar to that at the rotor exit. Thus, it appeared that the stator row provided little attenuation of the distortion of the flow out of the rotor.

Fan Back Pressure

The fan stage was designed with the assumption that the static pressure at the exit of both the stator row and the duct would be equal to the ambient pressure (essentially equal annular areas at stator and duct exits). However, this was not found to be the case. The fan stage experienced a wide variation in back pressure over the test range of operation. Variations in stage back pressure during crossflow can alter the operating point of the stage and therefore the magnitude of the stage thrust.

The variation in local static pressure ratio p/p_0 at various locations in the exit of the fan assembly under static conditions without exit louvers is shown in Fig. 12 as a function of rotor corrected tip speed. The figure reveals below-ambient pressures throughout, with exit pressures decreasing from the outer surface of the fan passage to the center of the turbine base. The reduced turbine base pressure is not unexpected since it is known from previous model tests of short annular nozzles (e.g., Ref. 16) that an annular axial discharge would tend to produce below-ambient base pressures (base flow problem). The observed below-ambient base pressures were believed to be due basically to the diffusion of the relatively high turbine discharge velocity (about 30% greater than the fan duct exit velocity).

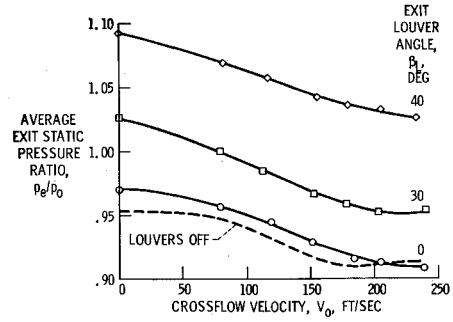

Fig. 13 Fan duct exit static pressure in crossflow—design tip speed; zero angle of attack.

The effect of crossflow velocity and louver position on fan duct exit static pressure ratio, p_e/p_0, is illustrated in Fig. 13. Variations are presented for the average of the duct hub and tip static pressure values at design tip speed. The expected increase in duct exit static pressure was observed as louver deflection angle was increased (i.e., louver exit flow area was decreased). However, increasing crossflow velocity produced a decrease in duct exit static pressure for all louver configurations. This latter trend is interpreted as indicating some form of interaction effect between the discharge streams from the fan and the crossflow airstream.

It was conjectured that a likely cause of the reduced fan exit static pressure was the propagation of the low turbine base pressure into the fan flow. This interpretation was explored by installing a 6-in.-long cylindrical separator between the fan and turbine discharge flows. Tests then revealed that the separation of the fan and turbine discharge flows did indeed result in an increase in the fan exit static pressure (up to the ambient value for the static case at design speed). However, the decrease in fan exit static pressure with increasing crossflow velocity persisted. This further verified the hypothesis of a discharge flow/crossflow interaction effect on fan back pressure.

Performance Maps

In order to evaluate the relative contributing effects of inlet flow distortion and exit back pressure ratio on fan performance in crossflow, it was helpful to define a basic performance map of the fan stage. Such a stage map without crossflow was obtained by attaching a remotely-actuated throttling device to the rear surface of the fan. The outer member of the throttle contained a diffusing section to achieve the lower values of exit static pressure. A conical throttle plug was supported by a cylindrical member which was fastened to the hub section of the fan. The cylinder separated the turbine and fan exhausts.

From the standpoint of the aircraft application, the most important propulsion parameters are fan thrust and input power. Consequently, the static performance map was defined in terms of corrected fan thrust (divided by inlet frontal area based on rotor tip diameter) and corresponding fan power input. The map for fan stage thrust is shown in Fig. 14. The average duct exit static pressure ratio, p_e/p_0, was chosen as the independent variable because it provided a direct assessment of the fan stage back pressure for this fan design. The static performance map of Fig. 14 shows the data obtained using the exit louvers as well as the throttle plug. A comparison between the basic range characteristics of the fan stage and the back pressure variation imposed by the louvers (or any other thrust vectoring or spoiling device) indicates the operating match between the fan stage and the exit device.

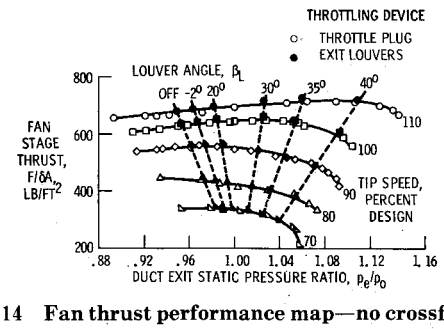

Fig. 14 Fan thrust performance map—no crossflow.

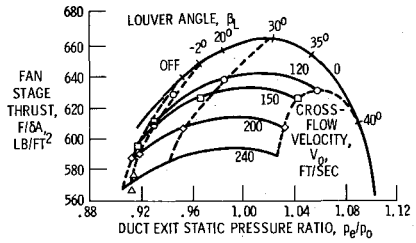

Fig. 15 Fan thrust performance map in crossflow—design tip speed; zero angle of attack.

The map of Fig. 14 clearly shows the over-all effect of fan back-pressure variations on fan stage static thrust. Thrust vectoring with louvers at design speed tended to first increase and then decrease thrust. At lower levels of tip speed, fan stage thrust tended to decrease as back pressure was increased for all values of louver position. A relatively good operating match appears to have been achieved between the louvers and the fan stage for this particular configuration.

A fan thrust map in crossflow was determined as shown in Fig. 15 for the test conditions of design tip speed and zero wing angle of attack. The upper curve is the variation in thrust obtained for the static case (no crossflow) as shown in Fig. 14. Locations corresponding to the various louver positions are given on this curve. Corresponding thrust/exit pressure curves were then constructed from the data obtained over a range of crossflow velocities. The crossflow curves appear to be similar in form to the static thrust variation. This was taken to indicate that the back pressure effect on fan stage thrust due to louver deflection in crossflow was essentially the same as that due to conventional outlet duct throttling. However, it is not apparent whether the static thrust map can be used quantitatively to establish the relative contributions of the inflow distortion effects and the back pressure variations to the observed change in stage thrust as crossflow velocity is increased for a given louver position.

Finally, since a lift fan is likely to be required to operate over a range of tip speeds, a thrust envelope map can be established as illustrated in Fig. 16 for 70% and 100% design tip speed for the static case and a crossflow case. Corresponding crossflow maps for fan power input can also be established.

Summary and Concluding Remarks

Fan thrust variations in crossflow were found to be the result of the effects of inflow distortion and stage back

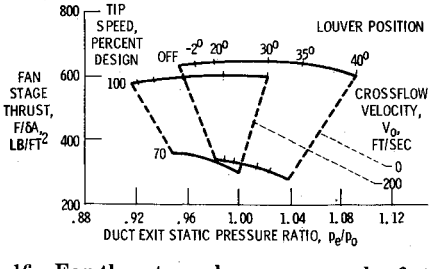

Fig. 16 Fan thrust envelope—zero angle of attack.

pressure variations induced by the crossflow. Inflow distortion affected fan performance primarily by losses in total pressure across the rotor and stator blade rows arising from circumferential variations in local blade inlet flow angle. Losses also occurred due to reduced weight flow and inlet total pressure arising from local separation of the boundary layer on the forward part of the inlet bellmouth. However, for the bellmouth design of the model fan tested, inlet flow separation did not appear to be a serious factor in thrust decline.

Fan stage back pressure (fan duct static pressure) was found to decrease with increasing rotor tip speed and increasing crossflow velocity, and to increase with increasing vectoring louver angle. Fan back pressure decrease with tip speed was established to be the result of the turbine base flow effect. Fan back pressure decrease with crossflow was conjectured to be the result of some interaction effect between the fan assembly discharge streams and the crossflow stream. Over-all performance of a fan installation in crossflow can readily be established from plots of fan thrust and power input against back-pressure ratio for constant tip speed over the range of crossflow velocities of interest.

It is recognized, of course, that the specific performance values obtained with the model fan in these tests may not be the same as for other lift fan designs and configurations. However, it is believed that the types of flow distributions observed with this fan are generally representative of the flow phenomena to be expected in lift fans in crossflow.

References

[1]Lieblein, S., "A Review of Lift Fan Propulsion Systems for Civil VTOL Transports," AIAA Paper 70-670, New York, June 1970.

[2]Lieblein, S., "Problem Areas for Lift Fan Propulsion for Civil VTOL Transports," *Bericht über das DGLR-Symposium VTOL-ANTRIEBE am 22/23, October 1970,* Munich, Germany, DLR Mitteilung 70-26, Dec. 1970, pp. 20–47.

[3]Grahame, W. E., "Aerodynamic Effects of Lift-Jet and Lift-Fan Inlets in Transition Flight," *Journal of Aircraft,* Vol. 6, No. 2, March-April 1969, pp. 150–155.

[4]Schaub, U. W., "Experimental Investigation of Flow Distortion in Fan-in-Wing Inlets," *Journal of Aircraft,* Vol. 5, No. 5, Sept.-Oct. 1968, pp. 473–478.

[5]Schaub, U. W., "Fan-in-Wing Aerodynamics: Experimental Assessment of Several Inlet Geometries," AIAA Paper 67-746, New York, Oct. 1967.

[6]Schaub, U. W. and Cockshutt, E. P., "Analytical and Experimental Studies of Normal Inlets with Special Reference to Fan-in-Wing VTOL Powerplants," *Proceedings of the 4th International Council of the Aeronautical Sciences Congress,* edited by R. R. Dexter, Spartan Books, 1965, pp. 519–553.

[7]Turner, R. C. and Sparkes, D. W., "Tests on a Simulated Lifting Fan System with Inlet Crossflow," R&M-3461, 1967, Aeronautical Research Council, Great Britain.

[8]Gregory, N., Raymer, W. G., and Love, E. M., "The Effect of Forward Speed on the Inlet Flow Distribution and Performance of a Lifting Fan Installed in a Wing," R&M-3388, 1965, Aeronautical Research Council, Great Britain.

[9]Hackett, J. E., "Wind Tunnel Tests on a Streamlined Fan-Lift Nacelle," R&M-3470, 1967, Aeronautical Research Council, Great Britain.

[10]Anon., "Results of Wind Tunnel Tests of a Full-Scale, Wing-Mounted Tip-Turbine-Driven Lift Fan," TRECOM-TR-63-21, AD-426785, Sept. 1963, General Electric Co., Cincinnati, Ohio.

[11]Przedpelski, Z. J., "Lift Fan Technology Studies," CR-761, 1967, NASA.

[12]Yuska, J. A., Diedrich, J. H., and Clough, N., "Llewis 9-Foot-By-15-Foot V/STOL Wind Tunnel," TMX-2305, 1971, NASA.

[13]Stockman, N. O. and Lieblein, S., "Theoretical Analysis of Flow in VTOL Lift Fan Inlets Without Crossflow," TN D-5065, 1969, NASA.

[14]Johnsen, I. A. and Bullock, R. O., "Aerodynamic Design of Axial-Flow Compressors," SP-36, 1965, NASA.

[15]Stockman, N. O., "Potential Flow Solutions for Inlets of VTOL Lift Fans and Engines," *Analytic Methods in Aircraft Aerodynamics,* AP-228, 1970, NASA, Washington, D.C., pp. 659–581.

[16]Kentfield, J. A. C., "Nozzles for Jet-Lift V/STOL Aircraft," *Journal of Aircraft,* Vol. 4, No. 4, July-Aug. 1967, pp. 283–291.